Combined Current Profile and Plasma Energy Control via Model Predictive Control in the EAST Tokamak

Hexiang Wang, William P. Wehner, Eugenio Schuster

Abstract— Extensive studies have shown that the toroidal current density profile, which is closely related to the poloidal magnetic flux profile, is a key factor to achieving advanced tokamak operating scenarios characterized by improved confinement and possible steady-state operation. In this work, a first-principles-driven, control-oriented model of the poloidal magnetic flux profile evolution is used to design a feedback controller via model predictive control (MPC). The aim of the feedback controller is to track a desired profile for the gradient of the poloidal magnetic flux by solving an optimal control problem in the presence of disturbances, non-modeled dynamics, and arbitrary initial conditions. The simulation results illustrate the capability of the proposed controller in dealing with perturbed initial conditions and disturbances.

I. INTRODUCTION

Nuclear fusion is the process by which two light nuclei fuse together to form one heavier nucleus. There is a mass fraction Δm that is converted into energy according to the mass-energy equivalence $\Delta E = \Delta mc^2$, where c is the speed of light in vacuum. In order for the fusion reaction to occur frequently enough, the nuclei must be heated to temperatures of about one hundred million degrees. At these temperatures, the reactants are in the plasma state and have enough kinetic energy to overcome the repelling electrostatic forces and to fuse. One of the most promising approaches to nuclear fusion is magnetic confinement, where magnetic fields are used to confine the plasma. A common solution is to close the magnetic field lines in on themselves, forming a torus as shown in Fig. 1. When the magnetic field is configured such that the field lines follow a helical path through the torus, i.e. they curve around in the poloidal direction (B_θ) as well as in the toroidal direction (B_ϕ), the confinement device is called a tokamak. Following any magnetic field line a number of times around the torus a closed flux tube is mapped, a so called magnetic-flux surface, which marks points of constant poloidal magnetic flux, Ψ [1].

Extensive research has been conducted to find high performance operating scenarios that are characterized by high fusion gain, good plasma confinement, plasma stability, and noninductively driven plasma current [2] with the goal of developing candidate scenarios for ITER [3], the next generation burning-plasma tokamak currently under construction. A key property that is related to both the stability and performance of the plasma is the magnetic poloidal flux profile (Ψ-profile), as well as its gradient and the inverse of its gradient. The design of control algorithms for the regulation of these profiles has recently attracted a great deal of attention [4]–[15]. Control approaches applied in this field are classified according to the use of a model. Non-model-
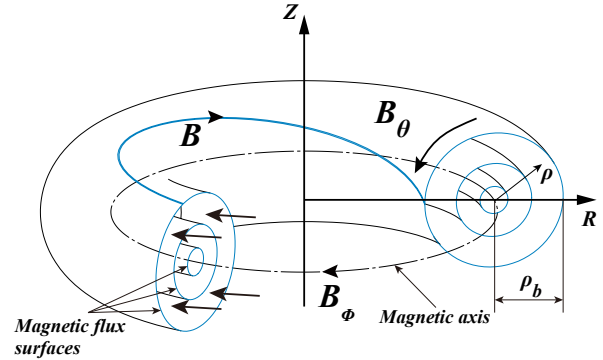

Fig. 1. Section view of the magnetic flux surfaces in a tokamak. The helical magnetic field B is composed by the poloidal (B_θ) and toroidal (B_ϕ) components. The limiting flux surface at the center of the plasma is called the magnetic axis. The coordinates (R, Z) define the radial and vertical dimensions in the poloidal plane of the tokamak. The coordinate ρ is used to index the magnetic flux surfaces.

based control mainly focuses on scalar parameters, such as feedback control of $q_0(t)$, the safety factor profile at the magnetic axis, $q_{min}(t)$, the minimum value of the safety factor profile, or the internal inductance, $l_i(t)$, a measure of the q-profile shape. The safety factor profile, $q(\hat{\rho}, t)$, is a measure of the pitch angle of the helical magnetic field lines and is a function of the inverse of the gradient of the poloidal flux profile. On the contrary, a model-based approach is needed to control the entire profile in order to achieve certain advanced tokamak operating scenarios.

In this work, a q-profile controller is designed for the EAST tokamak in China. The design is based on a first-principles-driven dynamic model of the poloidal magnetic profile evolution, which is governed by the magnetic diffusion equation (MDE). A finite difference method is applied to reduce the order of this partial differential equation (PDE). The goal of the feedback controller is to track a desired trajectory in presence of arbitrary initial conditions and injected disturbances. In this paper, the controller is designed by using the model predictive control (MPC) method, which is essentially a receding-horizon linear quadratic regulator (LQR) with constrained inputs. The control inputs are nonlinear combinations of the total plasma current, the non-inductive current-drive power, and the line-average plasma density. The advantage of MPC is that it takes into account the constraints on the control inputs during the design process, which saves the work of designing an anti-windup compensator to deal with the input constraints. On the other hand, in order to balance computational demand and control performance, efforts to tune design parameters such as horizon length, step size, and weights in the objective function are needed.

This paper is organized as follows. In Section II, a control-oriented physics-based model of the poloidal magnetic flux evolution is introduced. In Section III, a finite difference method is then applied to reduce the order of the infinite-dimensional model. In Section IV, the profile tracking problem is rewritten into an optimization problem for MPC design and an offset-free MPC is presented. Testing results for the proposed MPC are given in Section V. The results illustrate the capability of the offset-free MPC to handle arbitrary initial perturbations and injected disturbances. In Section VI, conclusions and future work are stated.

II. POLOIDAL MAGNETIC FLUX MODEL

A. Magnetic Diffusion Equation

The dynamics of the poloidal magnetic flux is governed by the magnetic diffusion equation (MDE) [16],

$$\frac{\partial \psi}{\partial t} = \frac{\eta(T_e)}{\mu_0 \rho_b^2 \hat{F}^2(\hat{\rho})} \frac{1}{\hat{\rho}} \frac{\partial}{\partial \hat{\rho}} \left(\hat{\rho} D_\psi(\hat{\rho}) \frac{\partial \psi}{\partial \hat{\rho}} \right) +$$
$$R_0 \hat{H}(\hat{\rho}) \eta(T_e) \frac{\langle \bar{j}_{NI} \cdot \bar{B} \rangle}{B_{\phi,0}}, \quad (1)$$

with two given boundary conditions,

$$\left. \frac{\partial \psi}{\partial \hat{\rho}} \right|_{\hat{\rho}=0} = 0, \qquad \left. \frac{\partial \psi}{\partial \hat{\rho}} \right|_{\hat{\rho}=1} = \frac{k}{2} I_p(t), \quad (2)$$

and where

$$D_\psi(\hat{\rho}) = \hat{F}(\hat{\rho}) \hat{H}(\hat{\rho}) \hat{G}(\hat{\rho}), \quad k = -\frac{\mu_0}{\pi} \frac{R_0}{\hat{G}(1)\hat{H}(1)}. \quad (3)$$

The poloidal stream function ψ is closely related to the poloidal flux ($\Psi = 2\pi\psi$). The spatial coordinate $\hat{\rho}$ is the normalized effective minor radius, which is denoted as $\hat{\rho} = \rho/\rho_b$, where ρ is the mean effective minor radius of the flux surface, i.e., $\pi B_{\phi,0} \rho^2 = \Phi$. The quantity Φ is the toroidal magnetic flux and ρ_b is the mean effective minor radius of the outermost closed magnetic flux surface. The quantity η is the plasma resistivity, T_e is the electron temperature, μ_0 is the vacuum permeability, R_0 is the major radius of the tokamak, $\langle \bar{j}_{NI} \cdot \bar{B} \rangle / B_{\phi,0}$ is the noninductive current-drive, $I_p(t)$ is the total plasma current, $\hat{F}, \hat{H}, \hat{G}$ are geometric factors related to the magnetic configuration of a specified plasma equilibrium and particle collisionality within the plasma. The safety factor q, which is related to the toroidal current density, is written as

$$q = -\frac{d\Phi}{d\Psi} = -\frac{B_{\phi,0} \rho_b^2 \hat{\rho}}{\partial \psi / \partial \hat{\rho}}. \quad (4)$$

Since the safety factor is inversely proportional to the spatial derivative of the poloidal magnetic flux, we define $\theta \triangleq \frac{\partial \psi}{\partial \hat{\rho}}$, and choose θ as controlled variable.

In addition, the volume-averaged plasma stored energy is modeled by a zero-dimensional balance equation

$$\frac{dE}{dt} = -\frac{E}{\tau_E} + P_{tot}, \quad (5)$$

where τ_E is the global energy confinement time. In this work, an L-mode (low confinement) energy confinement scaling law is used ($\tau_E \propto I_p^{0.96} P_{tot}^{-0.73} \bar{n}_e^{0.4}$) [17], where $\bar{n}_e$ is the line-average electron density ($\bar{n}_e(t) = \int_0^1 n_e(\hat{\rho}, t) d\hat{\rho}$). The quantity P_{tot} is the total power injected into the plasma and is modeled as $P_{tot} = P_{ohm} + P_{aux} - P_{rad}$, where P_{ohm} is the ohmic power, P_{aux} is the total auxiliary heating and current-drive power, and P_{rad} is the radiation power. The auxiliary heating and current-drive power in the EAST tokamak is represented as

$$P_{aux} = \sum_{i=1}^{4} P_{NBI_i} + \sum_{i=1}^{2} P_{LH_i} + P_{IC}, \quad (6)$$

where P_{NBI_i} is the power of four individual neutral beam injectors (NBI), P_{LH_i} is the power of two individual lower hybrid launchers (LH), and P_{IC} is the power of an ion cyclotron source. The current generated by the ion cyclotron is negligible, i.e. IC is considered as a heating source only.

B. Electron Density

In this work, the electron density $n_e(\hat{\rho}, t)$ is modeled as

$$n_e(\hat{\rho}, t) = n_e^{prof}(\hat{\rho}) \bar{n}_e(t), \quad (7)$$

where n_e^{prof} is a reference electron density profile.

C. Electron Temperature

The electron temperature is modeled as

$$T_e(\hat{\rho}, t) = T_e^{prof}(\hat{\rho}) I_p(t)^\alpha P_{tot}(t)^\gamma \bar{n}_e(t)^\kappa, \quad (8)$$

where T_e^{prof} is a reference temperature profile. The characteristic thermal diffusion time in the plasma is much faster than the characteristic resistive diffusion time. Therefore the temperature is always in quasi-equilibrium on the timescale of the current evolution. Based on (5), in quasi-equilibrium the volume-averaged plasma stored energy satisfies,

$$\frac{E}{\tau_E} = \frac{3\langle n_e \rangle_V \langle T_e \rangle_V V_p}{\tau_E} = P_{tot}, \quad (9)$$

where $\langle \cdot \rangle_V$ denotes the volume-average operation $\frac{\int_V (\cdot) dV}{V_p}$, V is the volume enclosed by a magnetic flux surface, and V_p is the total plasma volume. We have assumed, as an approximation, equal electron and ion temperatures and densities, i.e. $T_e(\hat{\rho}, t) = T_i(\hat{\rho}, t)$ and $n_e(\hat{\rho}, t) = n_i(\hat{\rho}, t)$, where $T_i(\hat{\rho}, t)$ and $n_i(\hat{\rho}, t)$ are the ion temperature and density profiles, respectively. By substituting (8) into (9), we have

$$\tau_E \propto I_p(t)^\alpha P_{tot}(t)^{(\gamma-1)} \bar{n}_e(t)^{(1+\kappa)}. \quad (10)$$

Therefore, the constants α, γ, κ in (8) are chosen to make (10) consistent with the energy confinement scaling law used in (5), which results in $\alpha = 0.96$, $\gamma = 0.27$, and $\kappa = -0.6$.

D. Plasma Resistivity

Following Spitzer resistivity model, the plasma resistivity $\eta(T_e)$ scales with the electron temperature as

$$\eta(\hat{\rho}, t) = \frac{k_{sp}(\hat{\rho}) Z_{eff}}{T_e(\hat{\rho}, t)^{3/2}}, \quad (11)$$

where k_{sp} is a constant and Z_{eff} is the effective atomic number of the ion species in the plasma.

E. Noninductive Current-drive

The total noninductive current-drive in this work is produced by the neutral beam injectors, the lower hybrid launchers, and the bootstrap current. It is expressed as

$$\frac{\langle \bar{j}_{NI} \cdot \bar{B} \rangle}{B_{\phi,0}} = \sum_{i=1}^{4} \frac{\langle \bar{j}_{NBI_i} \cdot \bar{B} \rangle}{B_{\phi,0}} + \sum_{i=1}^{2} \frac{\langle \bar{j}_{LH_i} \cdot \bar{B} \rangle}{B_{\phi,0}} + \frac{\langle \bar{j}_{BS} \cdot \bar{B} \rangle}{B_{\phi,0}}, \tag{12}$$

where $\bar{j}_{NBI_i}$ is the noninductive current generated by four individual neutral beam injectors, $\bar{j}_{LH_i}$ is the noninductive current generated by two individual lower hybrid launchers, and $\bar{j}_{BS}$ is the noninductive current generated by the bootstrap effect (modeled as in [18]).

1) Auxiliary Current-drive: We model each auxiliary noninductive current-source as

$$\frac{\langle \bar{j}_i \cdot \bar{B} \rangle}{B_{\phi,0}}(\hat{\rho}, t) = j_i^{dep}(\hat{\rho}) \frac{T_e(\hat{\rho}, t)^{\delta} P_i(t)}{\bar{n}_e(t)}. \tag{13}$$

The quantity $j_i^{dep}(\hat{\rho})$ is a reference deposition profile for each current-drive source, δ represents a current-drive efficiency factor, where δ is 0.5 for NBI and 1 for LH in this work to minimize the difference between the model prediction and experimental data from a reference shot, and P_i, $i \in \{NBI_1, NBI_2, NBI_3, NBI_4, LH_1, LH_2\}$ denotes the time varying power of each current-drive source.

2) Bootstrap Current-drive: This source is modeled as

$$\frac{\langle \bar{j}_{BS} \cdot \bar{B} \rangle}{B_{\phi,0}}(\hat{\rho}, t) = \frac{R_0}{\hat{F}(\hat{\rho})} \left(\frac{\partial \psi}{\partial \hat{\rho}} \right)^{-1} \left[2\mathcal{L}_{31}(\hat{\rho}) T_e \frac{\partial n_e}{\partial \hat{\rho}} + \{ 2\mathcal{L}_{31}(\hat{\rho}) + \mathcal{L}_{32}(\hat{\rho}) + \alpha(\hat{\rho})\mathcal{L}_{34}(\hat{\rho}) \} n_e \frac{\partial T_e}{\partial \hat{\rho}} \right], \tag{14}$$

where $\mathcal{L}_{31}(\hat{\rho}), \mathcal{L}_{32}(\hat{\rho}), \mathcal{L}_{34}(\hat{\rho})$ and $\alpha(\hat{\rho})$ depend on the magnetic configuration of a particular plasma equilibrium.

III. CONTROL-ORIENTED MODEL

Eight physical actuators are considered in this work, i.e.

$$u_{phy} = [I_p, P_{NBI_1}, P_{NBI_2}, P_{NBI_3}, P_{NBI_4}, P_{LH_1}, P_{LH_2}, P_{IC}].$$

Control of the electron density is challenging in practice, so we consider the line-average electron density as a measurable quantity instead of as an actuator. By substituting the resistivity model from (11) and the noninductive current-drive models from (13)–(14) into the MDE equation (1), we can write the MDE equation as

$$\frac{\partial \psi}{\partial t} = \left(C_{f_1} \frac{\partial \psi}{\partial \hat{\rho}} + C_{f_2} \frac{\partial^2 \psi}{\partial \hat{\rho}^2} \right) u_{diff} + \sum_i C_{j_i} u_{j_i} + C_{j_{BS}} \left(\frac{\partial \psi}{\partial \hat{\rho}} \right)^{-1} u_{j_{BS}}, \tag{15}$$

where

$$C_{f_1}(\hat{\rho}) = \frac{k_{sp}(\hat{\rho}) Z_{eff} \mu_0^{-1} \rho_b^{-2} \hat{F}^{-2}}{(k_{T_e}^{prof}(\hat{\rho}) T_e^{prof}(\hat{\rho}))^{1.5}} \left(\frac{D_\psi}{\hat{\rho}} + \frac{dD_\psi}{d\hat{\rho}} \right), \tag{16}$$

$$C_{f_2}(\hat{\rho}) = \frac{k_{sp}(\hat{\rho}) Z_{eff} \mu_0^{-1} \rho_b^{-2} \hat{F}^{-2}}{(k_{T_e}^{prof}(\hat{\rho}) T_e^{prof}(\hat{\rho}))^{1.5}} D_\psi, \tag{17}$$

$$u_{diff}(t) = \sqrt{I_p(t)^{-3\alpha} P_{tot}(t)^{-3\gamma} \bar{n}_e(t)^{-3\kappa}}, \tag{18}$$

$$C_{j_i} = \frac{R_0 \hat{H} k_{sp}(\hat{\rho}) Z_{eff} k_i(\hat{\rho}) j_i^{dep}(\hat{\rho})}{(k_{T_e}^{prof}(\hat{\rho}) T_e^{prof}(\hat{\rho}))^{(1.5-\delta)}}, \tag{19}$$

$$u_{j_i}(t) = (I_p(t)^\alpha P_{tot}(t)^\gamma)^{(\delta - 1.5)} \bar{n}_e(t)^{(\kappa(\delta - 1.5) - 1)} P_i(t), \tag{20}$$

with $i \in \{NBI_{1-4}, LH_{1,2}\}$ and

$$C_{j_{BS}} = \frac{R_0^2 \hat{H} k_{sp}(\hat{\rho})}{\hat{F} Z_{eff}^{-1} k_{JkeV}^{-1}} \left[\frac{2\mathcal{L}_{31}(\hat{\rho}) \dfrac{dn_e^{prof}(\hat{\rho})}{d\hat{\rho}}}{(k_{T_e}^{prof}(\hat{\rho}) T_e^{prof}(\hat{\rho}))^{0.5}} + \frac{[2\mathcal{L}_{31}(\hat{\rho}) + \mathcal{L}_{32}(\hat{\rho}) + \alpha(\hat{\rho})\mathcal{L}_{34}(\hat{\rho})] n_e^{prof}(\hat{\rho})}{k_{T_e}^{prof}(\hat{\rho})^{0.5} T_e^{prof}(\hat{\rho})^{0.5}} \cdot \left(\frac{1}{k_{T_e}^{prof}(\hat{\rho})} \frac{dk_{T_e}^{prof}(\hat{\rho})}{d\hat{\rho}} + \frac{1}{T_e^{prof}(\hat{\rho})} \frac{dT_e^{prof}(\hat{\rho})}{d\hat{\rho}} \right) \right], \tag{21}$$

$$u_{j_{BS}} = I_p(t)^{-0.5\alpha} P_{tot}(t)^{-0.5\gamma} \bar{n}_e(t)^{1 - 0.5\kappa}. \tag{22}$$

Similarly, the plasma energy equation can be written as

$$\frac{dE}{dt} = C_E E u_E + P_{tot} \triangleq f_E, \tag{23}$$

$$u_E = I_p(t)^{-0.96} P_{tot}(t)^{0.73} \bar{n}_e(t)^{-0.4}, \tag{24}$$

where C_E is a constant. The overall control input is

$$u = [P_{tot}, u_{diff}, u_{j_{NBI_1}}, u_{j_{NBI_2}}, u_{j_{NBI_3}}, u_{j_{NBI_4}}, u_{j_{LH_1}}, u_{j_{LH_2}}, u_{j_{BS}}, u_E]. \tag{25}$$

From the definition of P_{tot} and equations (18), (20), (22) and (24), it is possible to write the control inputs as a nonlinear function of the physical inputs, i.e., $u = g(u_{phy})$. By differentiating equation (15) with respect to $\hat{\rho}$, we obtain a PDE that describes the dynamics of $\theta \triangleq \partial \psi / \partial \hat{\rho}$,

$$\frac{\partial \theta}{\partial t} = \left[\frac{dC_{f_1}}{d\hat{\rho}} \theta + \left(\frac{dC_{f_2}}{d\hat{\rho}} + C_{f_1} \right) \frac{\partial \theta}{\partial \hat{\rho}} + C_{f_2} \frac{\partial^2 \theta}{\partial \hat{\rho}^2} \right] u_{diff} + \sum_i \frac{dC_{j_i}}{d\hat{\rho}} u_{j_i} + \left(\frac{dC_{j_{BS}}}{d\hat{\rho}} \frac{1}{\theta} - C_{j_{BS}} \frac{\partial \theta / \partial \hat{\rho}}{\theta^2} \right) u_{j_{BS}} \triangleq f_\theta, \tag{26}$$

with ($i \in \{NBI_{1-4}, LH_{1,2}\}$).

A. Model Reduction via Finite Difference

The infinite dimensional equation (26) is approximated by discretizing it spatially on a uniform grid that is defined as

$$\Delta \hat{\rho} = \frac{1}{n-1}, \quad \hat{\rho}_i = (i-1) \cdot \Delta \hat{\rho}, \quad i \in \{1, \cdots, n\}. \tag{27}$$

The variable θ at $\hat{\rho}_i$ can be represented as $\theta_i = \theta(\hat{\rho}_i, t)$. By defining $Z = [\theta_2, \cdots, \theta_{n-1}, E]$, and $F = [f_\theta, f_E]$, the discretized dynamics is modeled by $\dot{Z} = F(Z, u)$.

B. Error Modeling

To better facilitate control design, we further reduce the model by linearizing the plant F around a given trajectory (Z_{FF}, u_{FF}) satisfying $\dot{Z}_{FF} = F(Z_{FF}, u_{FF})$, i.e.,

$$\dot{Z} \approx F(Z_{FF}, u_{FF}) + \left. \frac{\partial F}{\partial Z} \right|_{(Z_{FF}, u_{FF})} (Z - Z_{FF}) + \left. \frac{\partial F}{\partial u} \right|_{(Z_{FF}, u_{FF})} (u - u_{FF}). \tag{28}$$
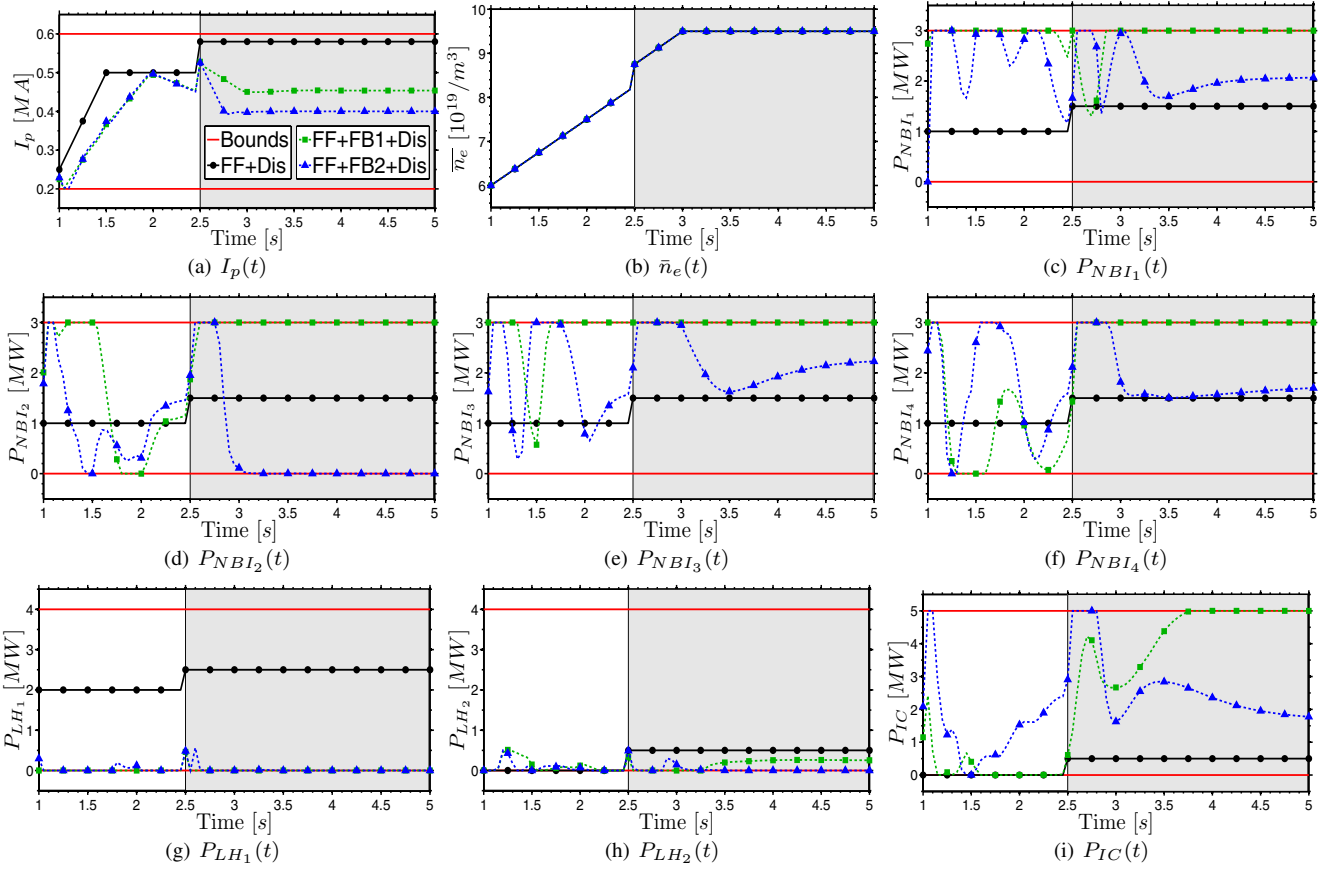
Fig. 2. Simulation testing of offset-free MPC: physical actuator trajectory comparison. FB1 represents a common MPC and FB2 is the proposed offset-free MPC. The shaded gray area denotes when the input disturbance is injected into the system. (a) $I_p(t)$. (b) $\bar{n}_e(t)$. (c) $P_{NBI_1}(t)$. (d) $P_{NBI_2}(t)$. (e) $P_{NBI_3}(t)$. (f) $P_{NBI_4}(t)$. (g) $P_{LH_1}(t)$. (h) $P_{LH_2}(t)$. (i) $P_{IC}(t)$.

By defining $\Delta_Z = Z - Z_{FF}$, $\Delta_u = u - u_{FF}$, and discretizing the model (28) on a temporal grid which is chosen as $t_j = j\Delta_t$, with $j \in \{0, 1, \cdots\}$, we can write the error model as

$$\frac{\Delta_Z^{j+1} - \Delta_Z^j}{\Delta_t} = A\Delta_Z^{j+1} + B\Delta_u^j, \qquad (29)$$

where A and B are the Jacobians $\partial F/\partial Z$ and $\partial F/\partial u$ evaluated at $(Z_{FF}(t_j), u_{FF}(t_j))$. Finally, we have

$$\Delta_Z^{j+1} = A_1\Delta_Z^j + B_1\Delta_u^j, \qquad (30)$$

where $A_1 = (I - A\Delta_t)^{-1}$ and $B_1 = (I - A\Delta_t)^{-1}B\Delta_t$.

IV. MODEL PREDICTIVE CONTROL

A. Principles of MPC

At every time t, the system model is used to predict the states up to time $t + hl$, where hl is the horizon length, based on measurements of the states at time t and a designed control sequence. A cost function weighting the feedback control effort and the tracking error between predicted states and desired states is minimized with respect to the control sequence. This defines an optimization problem in which input constraints can be added. The optimal control sequence is applied to the plant only until time $t + \Delta_t$, when new state measurements are obtained and the optimization problem is solved again by moving the prediction horizon up to time $t + \Delta_t + hl$ [19] and a new control sequence is obtained.

B. Control Input Constraints

Feedback control inputs Δ_u need to satisfy the actuator limits, which are

$$I_p^{min} - u_{FF}(1) \leq \Delta_u(1) \leq I_p^{max} - u_{FF}(1), \qquad (31)$$
$$P_{NBI1}^{min} - u_{FF}(2) \leq \Delta_u(2) \leq P_{NBI1}^{max} - u_{FF}(2), \qquad (32)$$
$$P_{NBI2}^{min} - u_{FF}(3) \leq \Delta_u(3) \leq P_{NBI2}^{max} - u_{FF}(3), \qquad (33)$$
$$P_{NBI3}^{min} - u_{FF}(4) \leq \Delta_u(4) \leq P_{NBI3}^{max} - u_{FF}(4), \qquad (34)$$
$$P_{NBI4}^{min} - u_{FF}(5) \leq \Delta_u(5) \leq P_{NBI4}^{max} - u_{FF}(5), \qquad (35)$$
$$P_{LH1}^{min} - u_{FF}(6) \leq \Delta_u(6) \leq P_{LH1}^{max} - u_{FF}(6), \qquad (36)$$
$$P_{LH2}^{min} - u_{FF}(7) \leq \Delta_u(7) \leq P_{LH2}^{max} - u_{FF}(7), \qquad (37)$$
$$P_{IC}^{min} - u_{FF}(8) \leq \Delta_u(8) \leq P_{IC}^{max} - u_{FF}(8), \qquad (38)$$
$$-I_{p,max}^d - \frac{du_{FF}(1)}{dt} \leq \frac{d\Delta_u(1)}{dt} \leq I_{p,max}^u - \frac{du_{FF}(1)}{dt}. \qquad (39)$$

where $(\cdot)^{min}$ indicates the minimum value of the corresponding inputs and $(\cdot)^{max}$ denotes the maximum value of the corresponding inputs. $I_{p,max}^d$ and $I_{p,max}^u$ represent the maximum I_p ramp-down and ramp-up rates, respectively. Additionally, Δ_u should satisfy

$$\Delta_u = H\Delta_{u_{phy}}, \quad H = \left.\frac{\partial g}{\partial u_{phy}}\right|_{u_{phy_{FF}}}. \qquad (40)$$
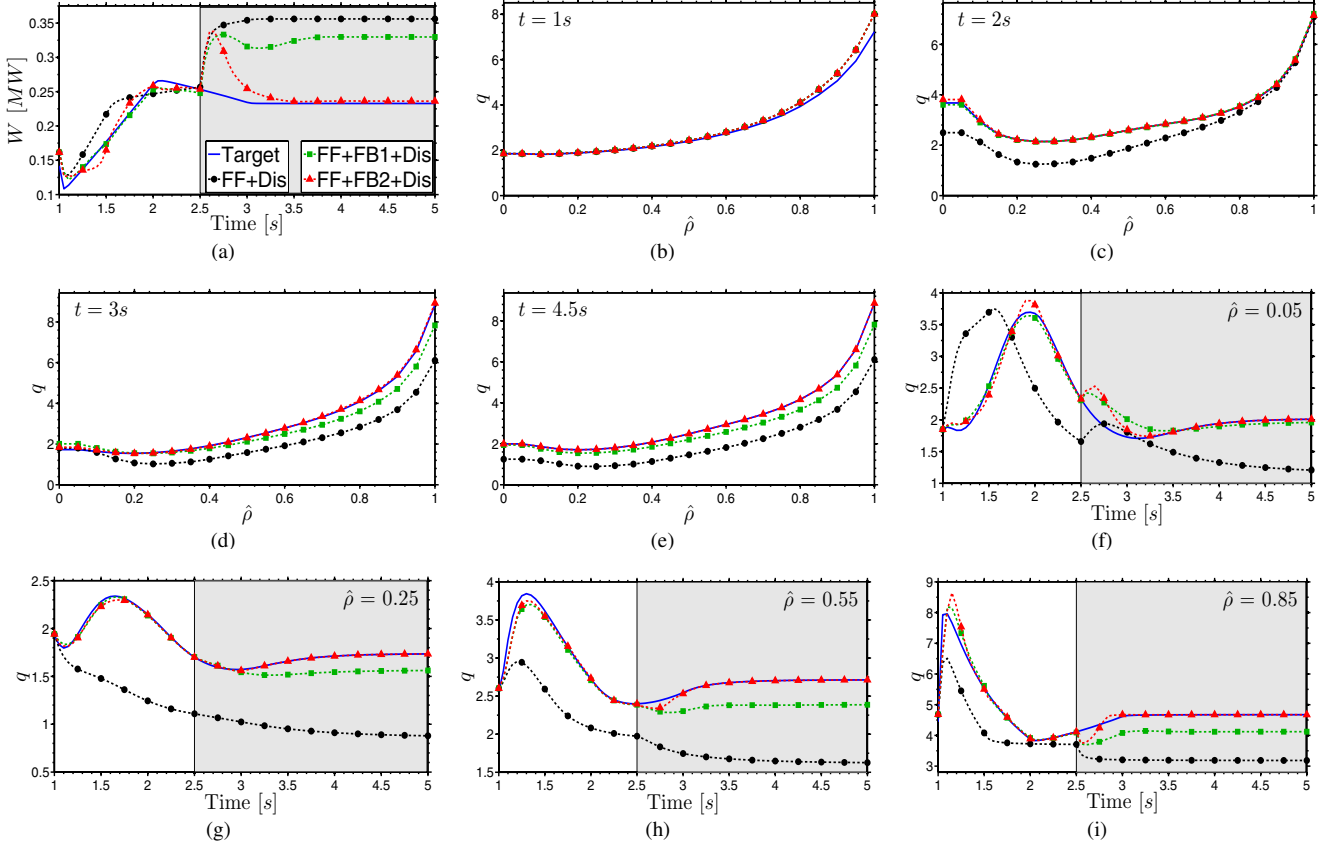
Fig. 3. Simulation testing of offset-free MPC: (a) plasma energy comparison, (b)-(e) q profile at $t = 1, 2, 3$ and $4.5s$, (f)-(i) q evolution at $\hat{\rho} = 0.05, 0.25, 0.55$ and 0.85. FB1 represents a common MPC and FB2 is the proposed offset-free MPC. The shaded gray area denotes when the input disturbance is injected into the system.

C. Offset-free MPC

MPC cannot guarantee offset-free tracking whenever there is a mismatch between the system model and the real plant or constant disturbances are present [20]. Two main approaches can be followed to tackle this problem. One is to estimate the disturbances by using an observer, the other is to write the system model in velocity form in order to incorporate integral action. In this work, the latter method is employed. By defining $d\Delta_Z^j = \Delta_Z^j - \Delta_Z^{j-1}$ and $d\Delta_u^j = \Delta_u^j - \Delta_u^{j-1}$, the system in velocity form is given as

$$d\Delta_Z^{j+k} = A_1 d\Delta_Z^{j+k-1} + B_1 d\Delta_u^{j+k-1}, \quad (41)$$

$$\Delta_Z^{j+k} = \Delta_Z^{j+k-1} + d\Delta_Z^{j+k}. \quad (42)$$

Similarly, the input constraints (40) can be shown as

$$H d\Delta_{u_{phy}}^{j+k-1} - d\Delta_u^{j+k-1} = \Delta_u^{j+k-2} - H\Delta_{u_{phy}}^{j+k-2}. \quad (43)$$

D. Formulation of Optimization Problem

By augmenting the state error increments shown in model (41), we define

$$X_j = \left[d\Delta_{u_{phy}}^j, d\Delta_u^j, d\Delta_Z^j \right] \in \mathbf{R}^{(n+17)}. \quad (44)$$

Since we want to minimize the tracking error and the feedback control effort over a receding horizon, we choose the variables for the optimization problem at $t = t_j$ as

$$X_{QP} = [X_j, X_{j+1}, \cdots, X_{j+hl-2}, X_{j+hl-1}]^T \in \mathbf{R}^{(n+17)hl}. \quad (45)$$

Let Z_{tar}^j be the desired state at $t = t_j$ and $\Delta_{Z_{tar}}^j = Z_{tar}^j - Z_{FF}^j$. The tracking error from $t = t_j$ to $t = t_{j+k}$ is

$$\Delta_Z^{j+k} - \Delta_{Z_{tar}}^{j+k} = \Delta_Z^{j-1} + \sum_{i=j}^{j+k} d\Delta_Z^i - \Delta_{Z_{tar}}^{j+k}. \quad (46)$$

We can write the discrete model of (41), (42), and (43) as $P X_{QP} = N$. At each time step, we have n-1 equations for $d\Delta_Z$ and 10 equations for $d\Delta_u$, which gives $P \in \mathbf{R}^{(n+9)hl \times (n+17)hl}, N \in \mathbf{R}^{(n+9)hl}$. Each one of the inequalities (31) - (39) has an upper bound and a lower bound, thus we have altogether 18 inequalities at each time step. They can be written as $P_I X_{QP} \leq N_I$, where $P_I \in \mathbf{R}^{18hl \times (n+17)hl}, N_I \in \mathbf{R}^{18hl}$.

The tracking problem is then written as

$$\min_{X_{QP}} \frac{1}{2} X_{QP}^T T^T Q T X_{QP} + M T X_{QP} \quad (47)$$

s.t. $P X_{QP} = N$ and $P_I X_{QP} \leq N_I$. T is a matrix that is used to convert $d\Delta_Z$ to Δ_Z and is written as

$$T = \left. \begin{bmatrix} I_{n+17} & \mathbf{0} & \mathbf{0} & \cdots & \mathbf{0} \\ G & I_{n+17} & \mathbf{0} & \cdots & \mathbf{0} \\ G & G & I_{n+17} & \ddots & \vdots \\ \vdots & \vdots & \ddots & \ddots & \mathbf{0} \\ G & G & \cdots & G & I_{n+17} \end{bmatrix} \right\} hl, \quad (48)$$

where the square matrix G is expressed as

$$G = \left[\begin{array}{cc} \mathbf{0} & \mathbf{0} \\ \mathbf{0} & I_{n-1} \end{array} \right], \qquad (49)$$

Q is a diagonal weighting matrix, and M is written as

$$M = ([\mathbf{0}, J_{1,n-1}, \cdots, \mathbf{0}, J_{1,n-1}]\Delta_Z^{j-1} -$$
$$[\mathbf{0}, \Delta_{tar}^{j}, \cdots, \mathbf{0}, \Delta_{tar}^{j+hl-1}])Q, \qquad (50)$$

where J is an all-ones matrix.

V. SIMULATION TESTING OF OFFSET-FREE MPC

In this section, the proposed offset-free MPC is tested through simulations based on the physics-based model of the plasma poloidal magnetic flux profile and plasma stored energy described in section II. Two feedforward-only simulations starting at $t = 1s$ with different sets of control inputs and different initial conditions are executed. The first feedforward-only simulation is used to generate target q-profile and E evolutions, while the second feedforward-only simulation is used to provide a trajectory for the error model. Closed-loop simulations are then carried out to track the target q-profile and E evolutions provided by the first feedforward-only simulation, with the initial conditions and feedforward control inputs used for the second feedforward-only simulation. An input disturbance u_d is injected at $t = 2.5s$, where $u_d^{I_p} = 0.08[MA]$, $u_d^{P_{NBI_{1-4}}} = 0.5[MW]$, $u_d^{\bar{n}_e} = 0.5[10^{19}/m^3]$, $u_d^{P_{LH_{1-2}}} = 0.5[MW]$, $u_d^{P_{IC}} = 0.5[MW]$. A common MPC and an offset-free MPC are tested for a comparison purpose. The test results are shown in Fig. 2 and Fig. 3. It can be seen from the figures, both the common MPC and the offset-free MPC are able to recover the desired q profile from a perturbed initial condition during the first two and half seconds. After the input disturbance is injected at $t = 2.5s$, the common MPC starts deviating from the target. On the contrary, the offset-free MPC is able to gradually reject the disturbance and maintain offset-free tracking. The offset-free MPC tends to have a larger overshoot compare to the common MPC. Both MPC controllers reduce the total plasma current to counteract the disturbance and to better match the q profile towards the plasma edge. Also, both MPC controllers manage to increase the power of NBI_1, which is the main on-axis current-drive, when q profile at $\hat{\rho} = 0.05$ are above the target value around $t = 2.75s$. However, due to the lack of integral action, the common MPC does not provide an overall offset-free tracking.

VI. CONCLUSION

In this paper, we present a model-based controller design for the gradient of the poloidal magnetic flux profile and the plasma stored energy on EAST. The controller is designed to track any set of target trajectories in presence of an initial state perturbation and input disturbances. A physics-based model is developed and linearized around a given trajectory. A reduced order system is then obtained through spatial discretization. The control problem is rewritten into an optimization problem with an augmented state composed of the tracking error and the feedback control signal. The proposed controller successfully tracks the given target trajectory. Plasma quantities related to magnetohydrodynamics (MHD) stabilities, such as the plasma β and Greenwald density limit, could be added to the set of state constrains for the formulated optimization problem. These constraint additions may play a critical role when testing the proposed MPC in real experiments on the EAST tokamak. A dedicated quadratic program solver, which exploits the structure of the inequality matrix P_I, is under development for upcoming experimental tests.

REFERENCES

[1] A. Pironti and M. Walker, "Fusion, tokamaks, and plasma control: an introduction and tutorial," *IEEE, Control Systems*, vol. 25, no. 5, pp. 30–43, 2005.

[2] T. Taylor *et al.*, "Physics of Advanced Tokamaks," *Plasma Phys. and Control. Fusion*, vol. 39, pp. B47–B73, 1997.

[3] ITER Organization, [Online]. Available: http://www.iter.org.

[4] Y. Ou, C. Xu, and E. Schuster, "Robust Control Design for the Poloidal Magnetic Flux Profile Evolution in the Presence of Model Uncertainties," *IEEE Transactions on Plasma Science*, vol. 38, pp. 375–382, 2010.

[5] ——, "Optimal Tracking Control of Current Profile in Tokamaks," *IEEE Transactions on Control Systems Technology*, vol. 19, pp. 432–441, 2011.

[6] C. Xu, Y. Ou, and E. Schuster, "Sequential Linear Quadratic Control of Bilinear Parabolic PDEs based on POD Model Reduction," *Automatica*, vol. 47, pp. 418–426, 2011.

[7] J. Barton and M. Boyer and W. Shi and E. Schuster, "Toroidal Current Profile Control During Low Confinement Mode Plasma Discharges in DIII-D via First-principles-driven Model-based Robust Control Synthesis," *Nucl. Fusion*, vol. 52, p. 123018, 2012.

[8] F. B. Argomedo *et al.*, "Lyapunov-based Distributed Control of the Safety-factor Profile in a Tokamak Plasma," *Nuclear Fusion*, vol. 53, no. 3, p. 033005, 2013.

[9] N. M. T. Vu *et al.*, "An IDA-PBC Approach for the Control of 1D Plasma Profile in Tokamaks," in *52nd IEEE Conference on Decision and Control*, 2013, pp. 4176–81.

[10] M. D. Boyer, J. E. Barton, E. Schuster *et al.*, "Backstepping Control of the Toroidal Plasma Current Profile in the DIII-D Tokamak," *IEEE Trans. Control Syst. Technol.*, vol. 22, no. 5, pp. 1725–1739, 2014.

[11] ——, "First-principles-driven Model-based Current Profile Control for the DIII-D Tokamak via LQI Optimal Control," *Plasma Phys. Control. Fusion*, vol. 55, p. 105007, 2013.

[12] M. Boyer and J. Barton and W. Shi and W. Wehner and E. Schuster, "Simultaneous Boundary and Distributed Feedback Control of the Current Profile in H-mode Discharges on DIII-D," in *19th IFAC World Congress*, 2014, pp. 1568–1573.

[13] O. Gaye *et al.*, "Sliding Mode Stabilization of the Current Profile in Tokamak Plasmas," in *50th IEEE Conference on Decision and Control (Orlando, FL, USA)*, 2011, pp. 2638–2643.

[14] Y. Ou, C. Xu, E. Schuster, T. C. Luce, J. R. Ferron, M. L. Walker, and D. A. Humphreys, "Receding-Horizon Optimal Control of the Current Profile Evolution During the Ramp-Up Phase of a Tokamak Discharge," *Control Engineering Practice*, vol. 19, pp. 22–31, 2011.

[15] E. Maljaars *et al.*, "Control of the Tokamak Safety Factor Profile with Time-varying Constraints using MPC," *Nuclear Fusion*, vol. 55, p. 023001, 2015.

[16] Y. Ou *et al.*, "Towards model-based current profile control at DIII-D," *Fusion Engineering and Design*, vol. 82, pp. 1153–1160, 2007.

[17] ITER Physics Basis Editors *et al.*, *Nuclear Fusion*, vol. 39, no. 12, pp. 2201–2215, 1999.

[18] O. Sauter, C. Angioni, and Y. R. Lin-Liu, "Neoclassical conductivity and bootstrap current formulas for general axisymmetric equilibria and arbitrary collisionality regime," *Physics of Plasmas*, vol. 6, no. 7, pp. 2834–2839, 1999.

[19] W. H. Kwon and S. Han, *Receding Horizon Control*. London, U.K.: Springer-Verlag, 2005.

[20] G. Pannocchia, "Offset-free tracking MPC: A tutorial review and comparison of different formulations," in *ECC15*, 2015, pp. 527–532.